Supporting Information for:

Minimalistic coarse-grained models to investigate the structure of biomimetic membranes

Małgorzata Kowalik[1,*], Allen B. Schantz[1,*], Abdullah Naqi[1], Yuexiao Shen[1,2], Ian Sines[1,3], Janna K. Maranas[1] and Manish Kumar[1,4,5]

[1] Department of Chemical Engineering, The Pennsylvania State University, University Park, PA 16802

[2] Department of Chemistry, University of California Berkeley, Berkeley, CA, 94704

[3] Surface Conditioning Business Unit, Saint Gobain, Northborough, MA, 01532

[4] Department of Civil and Environmental Engineering, The Pennsylvania State University, University Park, PA 16802

[5] Department of Biomedical Engineering, The Pennsylvania State University, University Park, PA 16802

* Contributed equally

Atomimistic simulations of 1,2-BD with different tacticity and up to 10% 1,4-BD impurities

Ideally, we want to reproduce EO-1,2-BD membrane structures using a minimalistic model containing only one bead representing each monomer. However, the polybutadiene produced via anionic polymerization has a number of complicating structural features; we must either account for these features with a more complex model or show that we can neglect or average out their influence on the melt structure. The first of these features is that the polybutadiene we synthesized contains 90% 1,2 monomers and 10% 1,4 monomers (shown via NMR), so that we should determine whether we can neglect the 1,4 impurities. Further, the 1,2-BD is atactic, so that we need to consider how the sequence of L and R isomers affects the bonded structure. Finally, the EO-1,2-BD polymers used in biomimetic membranes have degrees of polymerization 12-34 for the hydrophobic block, so that we should consider whether the structures might vary with degree of polymerization.

To examine these issues, we ran a series of short (5-ns) simulations using the NPT ensemble (P = 1atm, T = 323K for 1,2-BD and 300K for 1,4-BD) with timestep 0.5 fs and a Nose-Hoover thermostat and barostat with time constants 50 fs and 500 fs respectively. A higher temperature was used for 1,2-BD than 1,4-BD to ensure that the 1,2-BD was at least 50 K above its glass transition temperature of approximately 268-273 K compared to 166-178 K for 1,4-BD. 1,2-BD melt simulations were run using chains with degree of polymerization N = 9, 12, and 18 monomers to examine the influence of chain length. We also conducted simulations of cis 1,4-BD, trans 1,4-BD, and 90% 1,2-BD melts containing chains with N = 18 to examine the effect of 1,4-BD impurities. In all simulations containing atactic chains (1,2-BD or 90% 1,2-BD), each polymer chain in the simulation box was an independently generated random copolymer of the relevant

monomers (L 1,2-BD, R 1,2-BD, and when applicable cis 1,4-BD and trans 1,4-BD). To ensure a sufficient ensemble average, we ran melt simulations containing two different numbers of chains for the three 1,2-BD melts, and we observed no substantial differences in structural distribution functions upon increasing the number of chains (see **Figure S1**).

To judge whether we could use a minimalistic model containing only one bead type for polybutadiene (a 1,2-BD monomer whose bonded and nonbonded potential functions reflect an average over numerous atactic chains), we asked three questions about the deviations between the various polymer melts simulated. First, are the deviations between the different melts' radial, bond length, angle, and dihedral distributions (due to chain length or stereochemistry) greater than the differences between the same distributions for coarse-grained and all-atom simulations of a melt of 53 1,2-BD18 chains? If not, differences in all-atom structure will not meaningfully change the final CG potentials. Similarly, are the differences between the distribution functions for the various melts more different from each other than the deviations between CG and atomistic distributions commonly shown for published CG models based on atomistic simulations? We answered both these questions in the negative for 1,2-BD melts of various chain lengths and distributions of left-handed and right-handed isomers, as will be shown later. For melts containing 10% 1,4-BD impurities, we do see some differences in the bonded and nonbonded structure outside the resolution of the CG parameterization. If these differences will make a noticeable difference in membrane properties, we will need to account for them. To test this, we ask whether the average bonded structures for chains with and without 1,4 impurities will lead to end-to-end distances more than 1 nm different from each other, and thus create the possibility that the membrane thickness would be incorrect by an amount greater than the resolution of the cryo-TEM measurements that we use to validate the model. We answer this question in the negative (shown later), showing that a minimalistic model is appropriate.

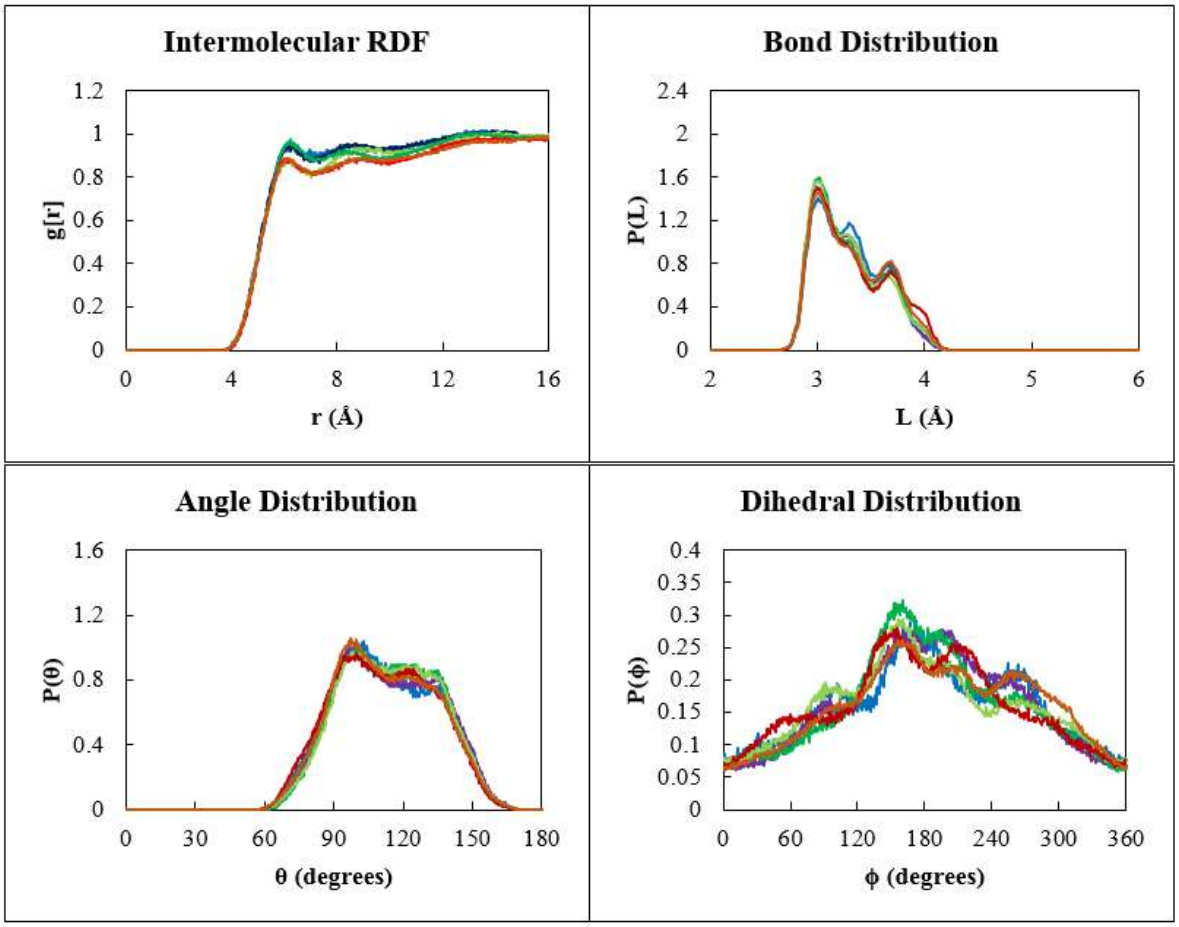

Figure S1: Radial distribution functions, bond length distributions, angle distributions, and dihedral distributions for melts of 1,2-BD chains with different degrees of polymerization and numbers of chains. Blue: $N_{monomer}$ = 9, n_{chain} = 27; purple: $N_{monomer}$ =9, n_{chain} = 64; dark green: $N_{monomer}$ = 12, n_{chain} = 27; light green: $N_{monomer}$ = 12, n_{chain} = 64; red: $N_{monomer}$ = 18, n_{chain} = 27; orange: $N_{monomer}$ = 18, n_{chain} = 64.

Based on **Figure S1**, it appears that the radial, bond, angle, and dihedral distributions are similar for various chain lengths and numbers of 1,2-BD chains. A preliminary CG model was developed via Iterative Boltzmann Inversion to reproduce the structure of the melt with the best statistics (n_{chain} = 53, $N_{monomer}$ = 18). In **Figure 2**, we compare the CG distributions to those of the target AA melt, and observe that their differences are similar to the deviations between the various AA 1,2-BD melt distributions.

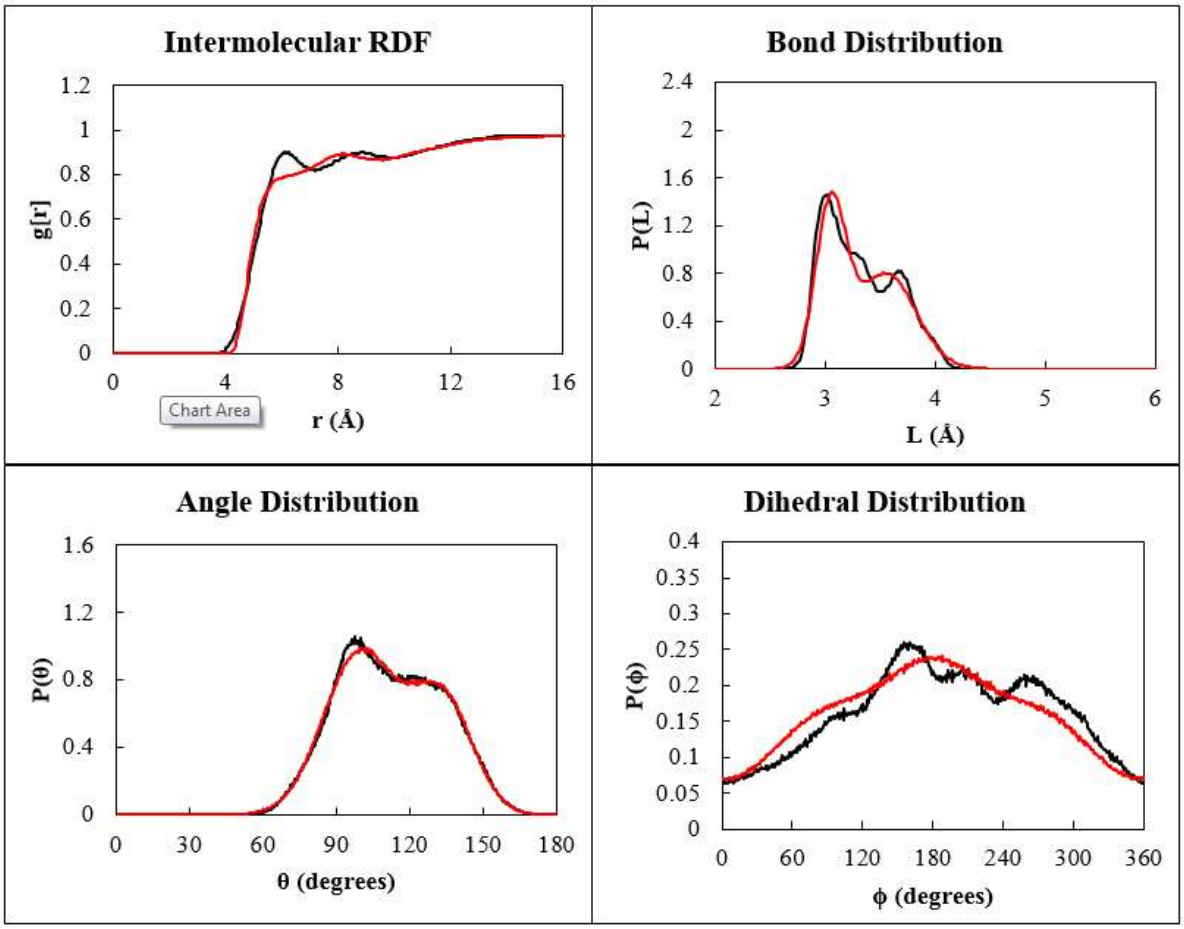

Figure S2: Comparison of atomistic and preliminary CG structural distribution functions for the 1,2-BD melt with 53 atactic, 18-monomer chains. Atomistic target distributions are shown in black, while distributions from the CG model are shown in red.

Because the deviations between the CG and AA distributions are similar to those due to degree of polymerization and between different ensembles of AA chains, we can safely use the same model for chains of different length and use an ensemble average rather than separate L and R isomer beads to account for stereochemistry. In **Figure S3**, we compare a simulated melt containing 27 randomly polymerized 90% 1,2-BD18 chains to the 100% 1,2-BD melts with $N_{monomer}$ = 9, 12, 18 and n_{chain} = 64, 64, and 53 (these melts are chosen because they have more chains and therefore better statistics than the 27-chain melts). We observe that these melts are structurally similar, although the 1,4-BD impurities slightly increase the number of long bonds and large angles.

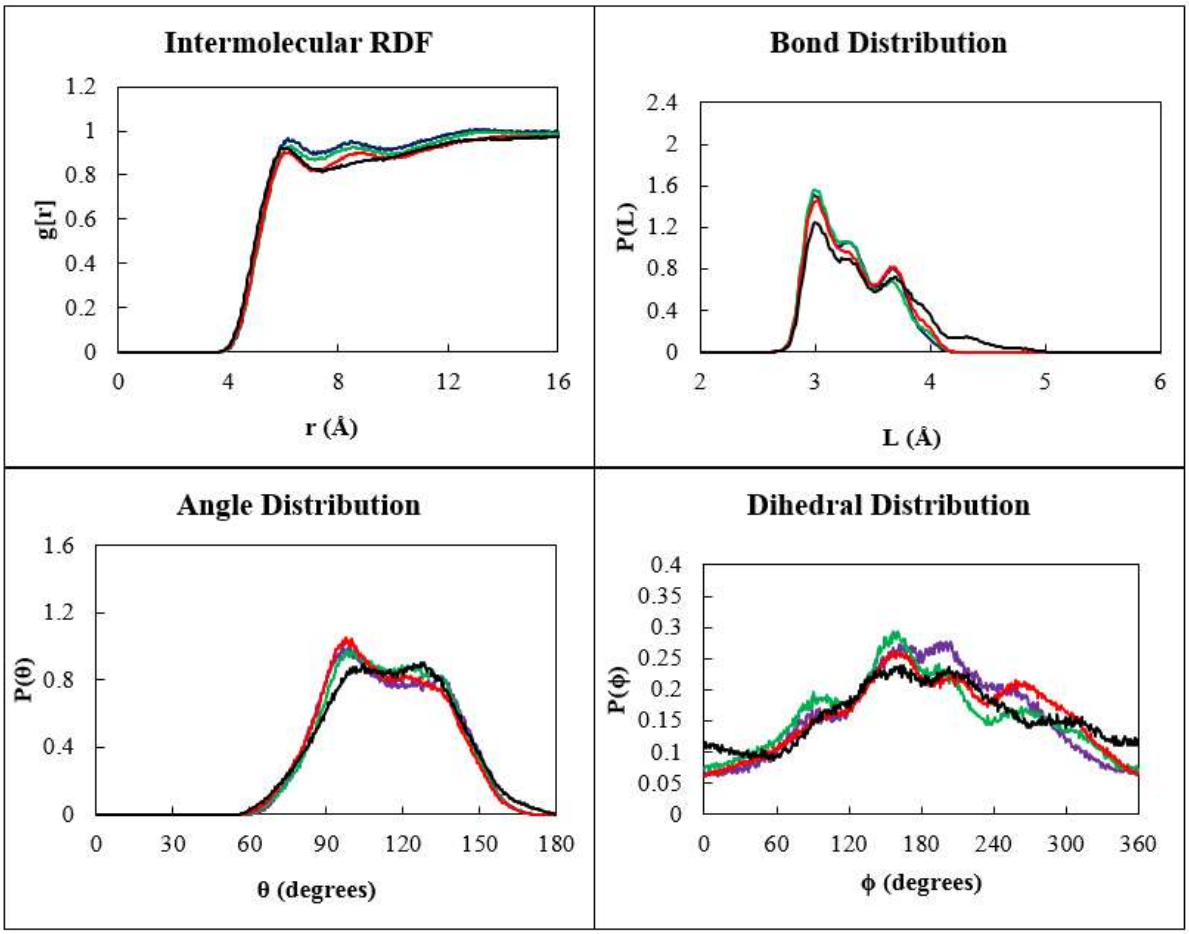

Figure S3: Atomistic distribution functions for a 1,2-BD melt of polymers containing 10% 1,4-BD impurities. Radial, bond, angle, and dihedral distributions for melts containing 1,4-BD impurities are compared to those without. Black lines correspond to a 90% 1,2-BD melt with n_{chain} = 27 and $N_{monomer}$ = 18. Colored lines correspond to 100% 1,2-BD: blue indicates n_{chain} = 64, $N_{monomer}$ = 9; green indicates n_{chain} = 64, $N_{monomer}$ = 12; and red indicates n_{chain} = 53, $N_{monomer}$ = 18.

To examine the reasons for the differences between the 90% and 100% 1,2-BD melts, we also simulated cis and trans 1,4-BD melts with n_{chain} = 27 and $N_{monomer}$ = 18. In the resulting distributions, we see that both cis and trans 1,4-BD have substantially longer bonds and wider angles between monomers than atactic 1,2-BD, leading to the differences between the 90% and 100% 1,2 bond and angle distributions (see **Figure S4**).

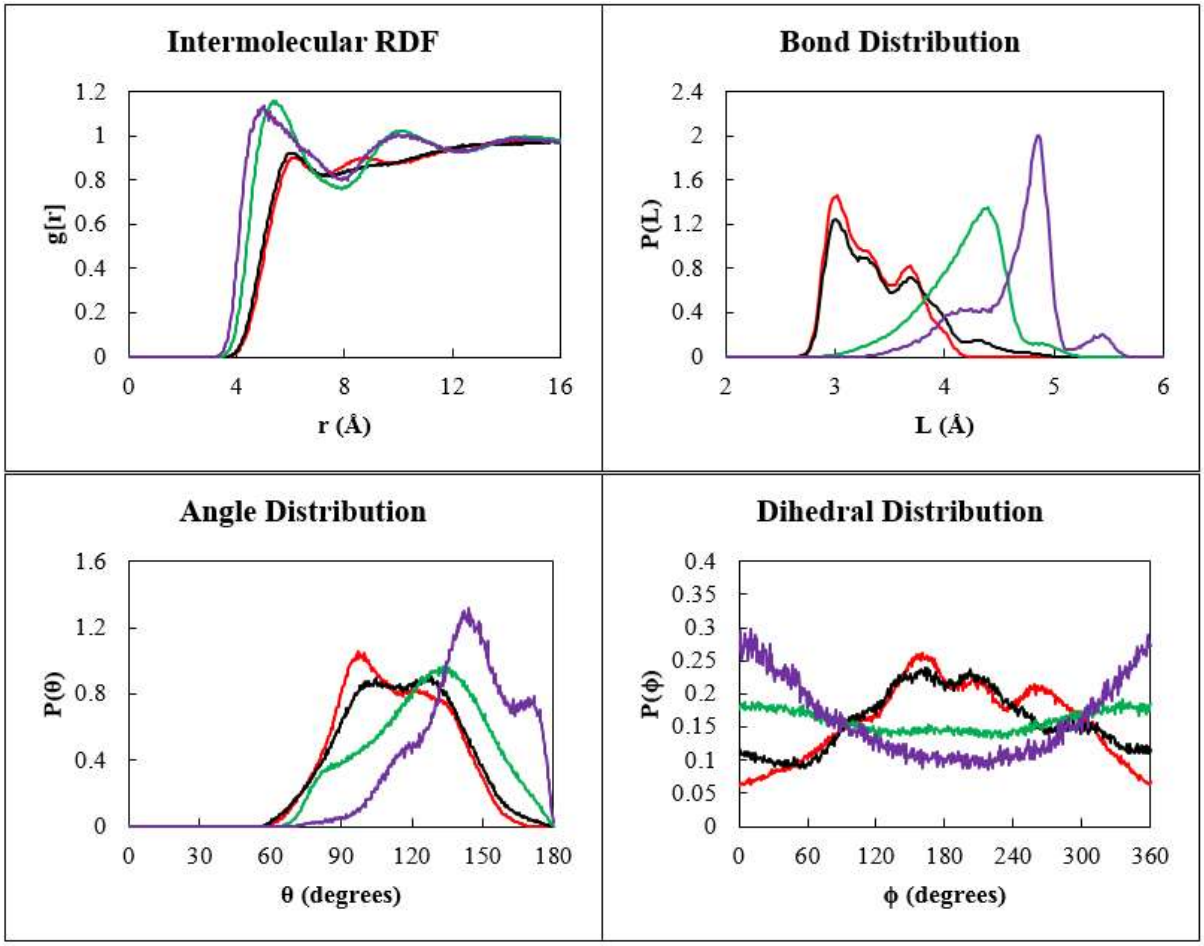

Figure S4: The butadiene isomers present in an atomistic melt simulation change the distribution functions. Distributions are shown for 1,2-BD (red), cis 1,4-BD (green), trans 1,4-BD (purple), and 90% 1,2-BD (black).

Using these distributions, we test whether the differences in the bonded structure of 100% and 90% 1,2-BD might result in a statistically significant difference between our simulations results and the experimental data (membrane thickness from cryo-TEM). Membrane thickness can be determined to within about 1 nm, and differences in membrane thickness will be less than differences between fully stretched chain lengths because the hydrophobic polymers are not fully extended – membrane core thickness is known to scale with the number of Kuhn monomers N as N^{α} $(1/2 \leq \alpha \leq 2/3)$[1] rather than as N^{1} (as it would for a fully extended chain). Therefore, we determine whether the average bonds and angles for 100% and 90% 1,2-BD would result in a difference of at least 1 nm between the end-to-end distances for fully stretched chains (all CG dihedrals in the trans conformation) for the longest BD block we simulate (BD37). Thus, if the end-to-end distances are within 1 nm, neglecting the 1,4 impurities cannot result in a statistically significant difference between the simulations and experimental data. This test shows that the synthetic impurities will cause a difference in membrane thickness no more than 1/10 the

resolution of the TEM measurements, so we can parameterize a CG model without taking these impurities into account (see **Table S1**).

Table S1: Calculation of the end-to-end distances for BD37 chains with and without 1,4 impurities. This distance is given by $d = N_{bond}*L_{bond}*\sin(\theta/2) = (N_{monomer} - 1) *L_{bond}*\sin(\theta/2)$.

	100% 1,2-BD	90% 1,2-BD
Average bond length [Å]	3.3	3.4
Average angle [degrees]	112	115
End-to-end distance [Å]	110	111
Difference/cryo-TEM resolution	0.1	

After conducting these tests, we decided to use the 53-chain 1,2-BD18 melt simulation as the target for our CG parameterization. To ensure that this system was well-equilibrated, we ran it for an additional 150 ns (requiring approximately 2400 hours or 100 days of simulation time with the computational resources available to us). The distribution functions stopped changing after approximately 60 ns, and the mean-squared displacement after 120 ns was about equal to the square of the BD18 chain's radius of gyration (about 10 Å), suggesting that each chain was able to sample a range of conformations, so that its local structure is likely to be equilibrated (**Figures S5** and **S6**). Thus, we believe that the average distributions calculated over the last 90 ns of this simulation represent an equilibrated system, and we use these distributions as a target for the final CG 1,2-BD model. Further, the fully equilibrated configurations are similar to those from the preliminary simulations, giving us confidence that although the nine melts used to determine that we can use a minimalistic model were not fully equilibrated, the conclusions we made about what variables to account for or ignore were reasonable. Although it would be more precise to run all nine melt simulations until they are well-equilibrated, with the computational resources available, we can run about 2 simulations at a time, so that running the other eight melt simulations for the same amount of time as for the 53-chain BD18 simulation would require approximately 400 days, which we do not consider a good use of our time and computer resources.

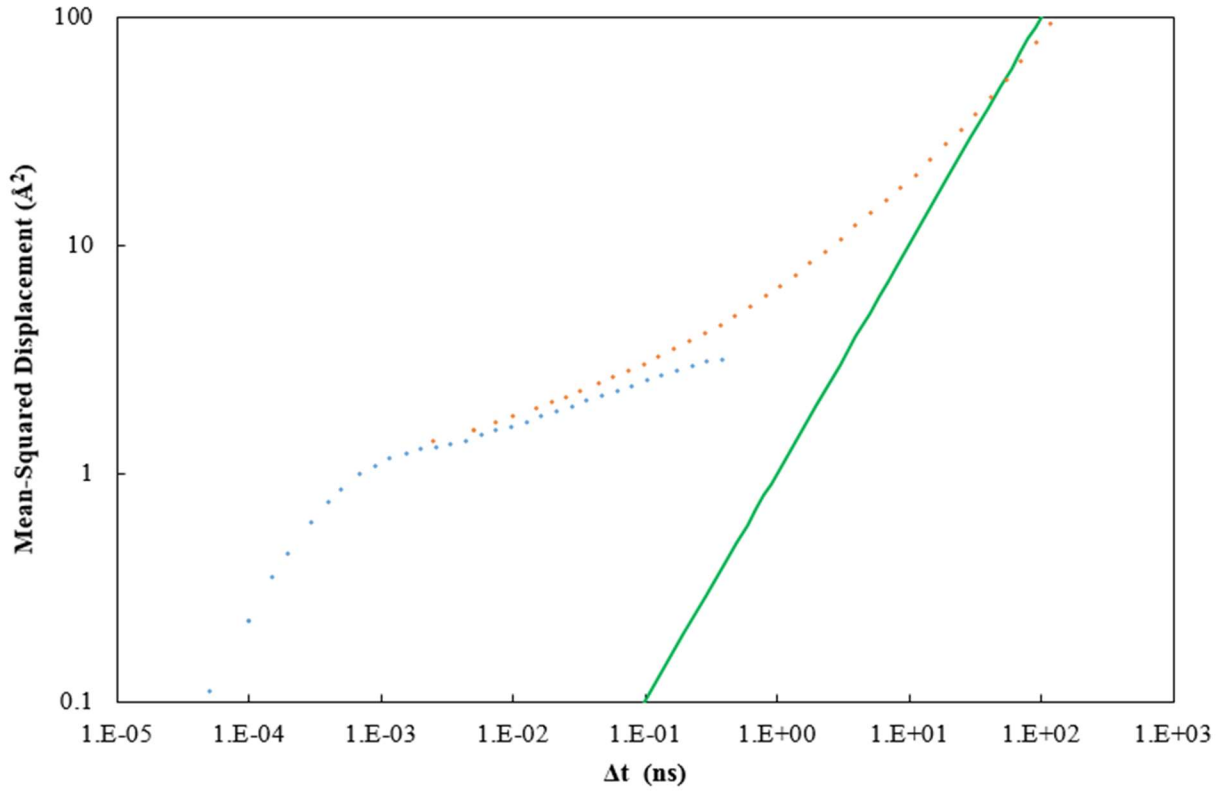

Figure S5: Mean-squared displacement (MSD) for an atomistic 1,2-BD18 melt simulation with n_{chain} = 53. MSD is calculated both for the 155 ns equilibration/data collection simulation (red diamonds) and for a 500 ps simulation during which atoms' coordinates were output more frequently, allowing us to calculate the MSD at smaller time increments (blue). The initial rise ($\Delta t < 10^{-3}$ ns) shows each atom exploring its local environment, the shallower slope from approximately 10^{-3} to 1 ns shows that motion is hindered by neighboring atoms, and the steeper rise at $\Delta t > 1$ ns shows that the atoms have escaped their local confinement and their motions are becoming closer to unhindered diffusion, which would result in a slope of 1 (green).

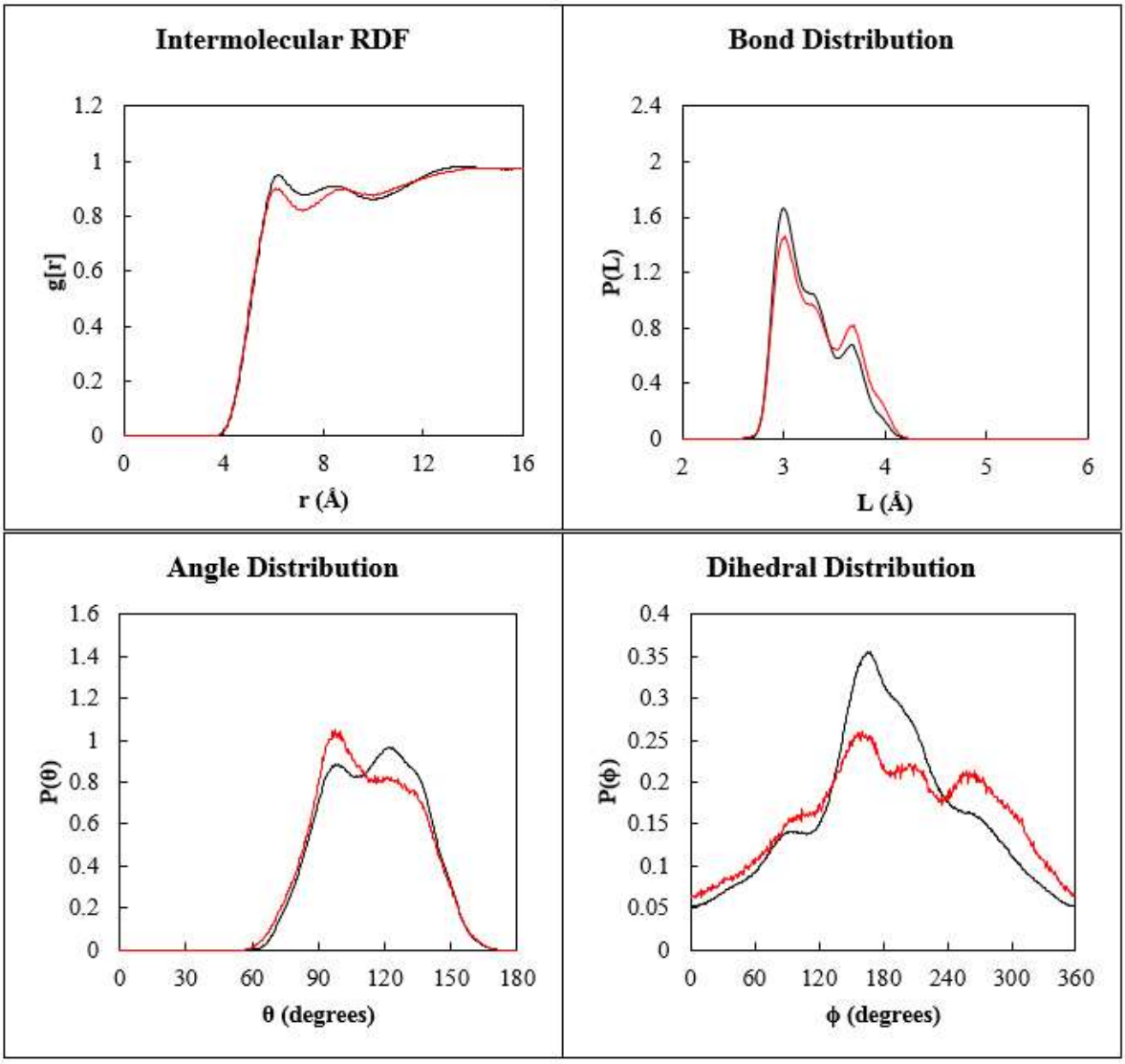

Figure S6: Radial, bond length, angle, and dihedral distributions for initial (5 ns) and equilibrated (60 ns equilibration, 95 ns production) melt simulations. Initial distributions are shown in red, while equilibrium distributions are shown in black.

Fluctuations of the membrane stress tensor

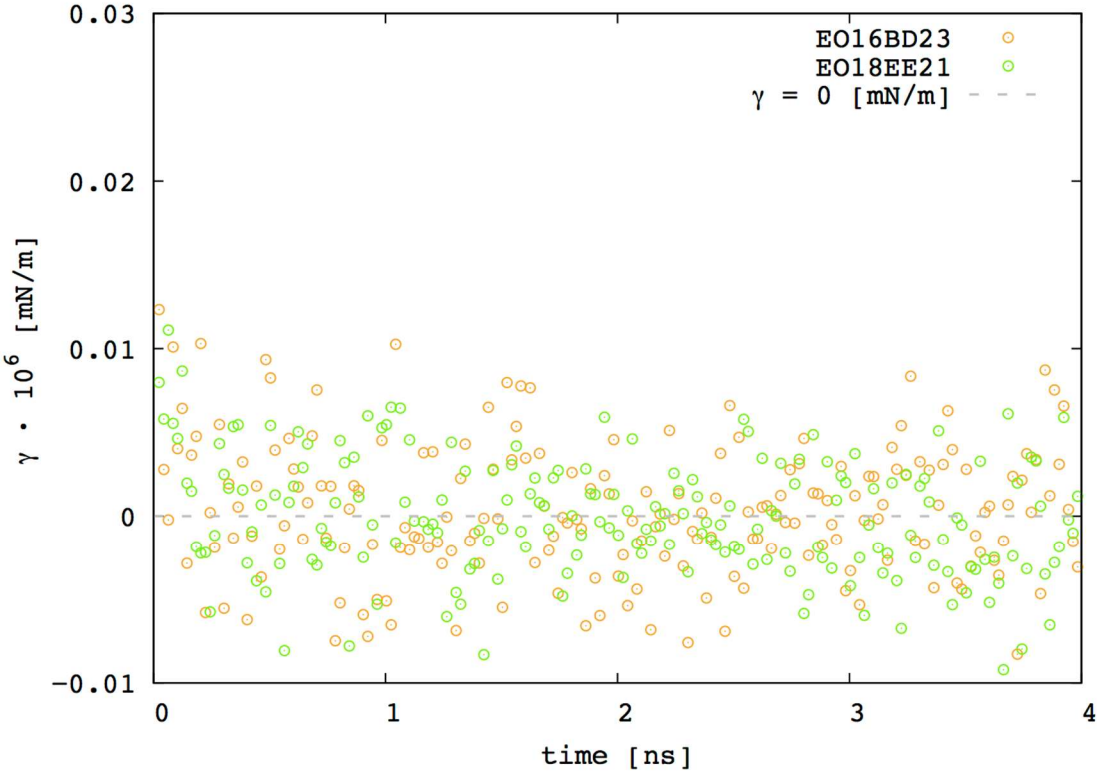

Figure S7: The stress tensor fluctuations for CG EO-EE membranes. We show the fluctuations of the stress tensor γ for two membranes: EO16-BD23 and EO18-EE21. Fluctuations around zero indicate that the barostats are maintaining the simulated membrane in a tensionless condition.

Bonded structure in vacuum and in the membrane

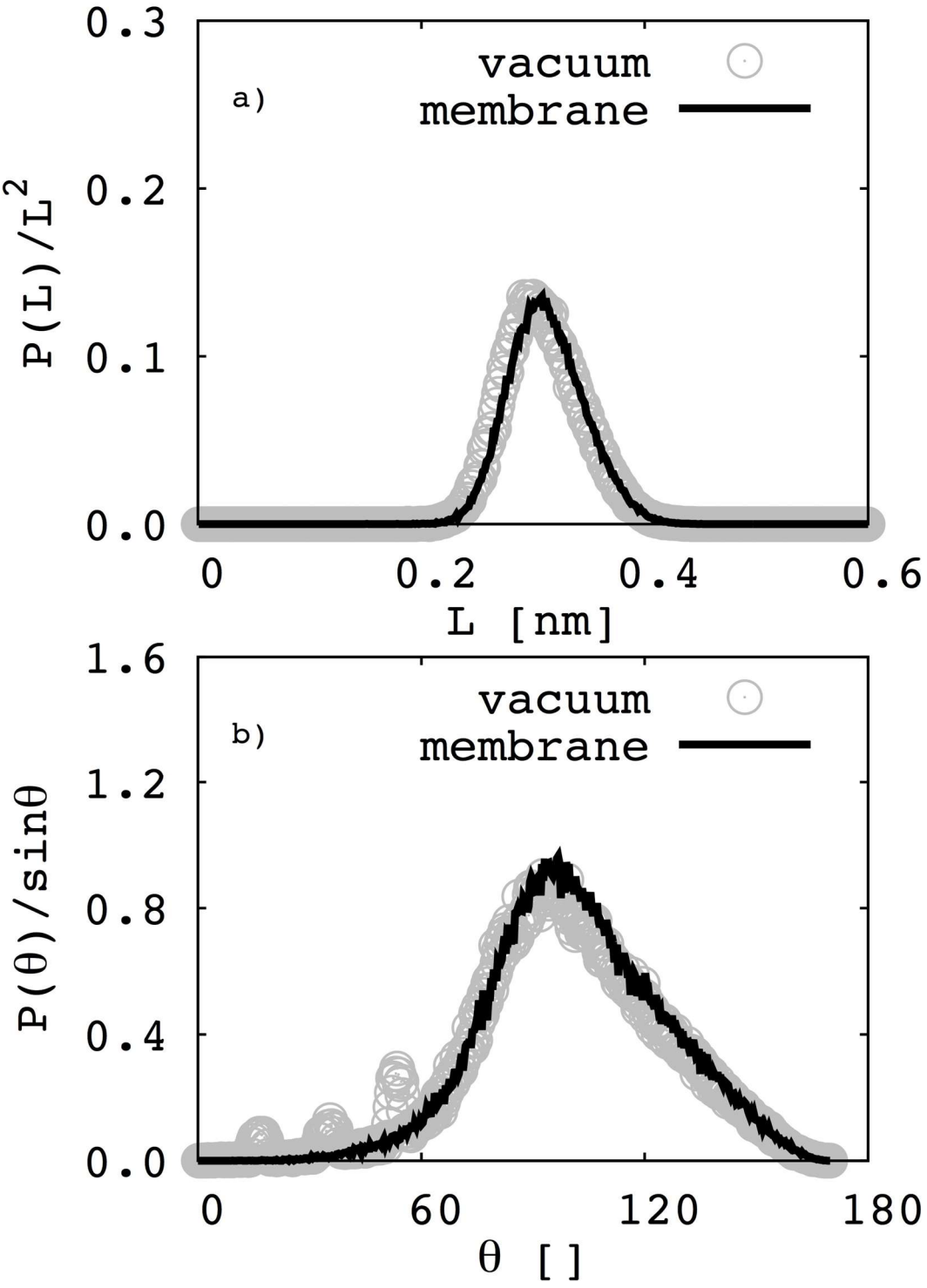

Figure S8: Probability distributions P(L) and P(θ) for the CG EO-EE junction bond length and EO-EE-EE junction angle. Distributions in the membrane and in vacuum are shown for EO18EE21.

Influence of the scaling factor λ on area/chain

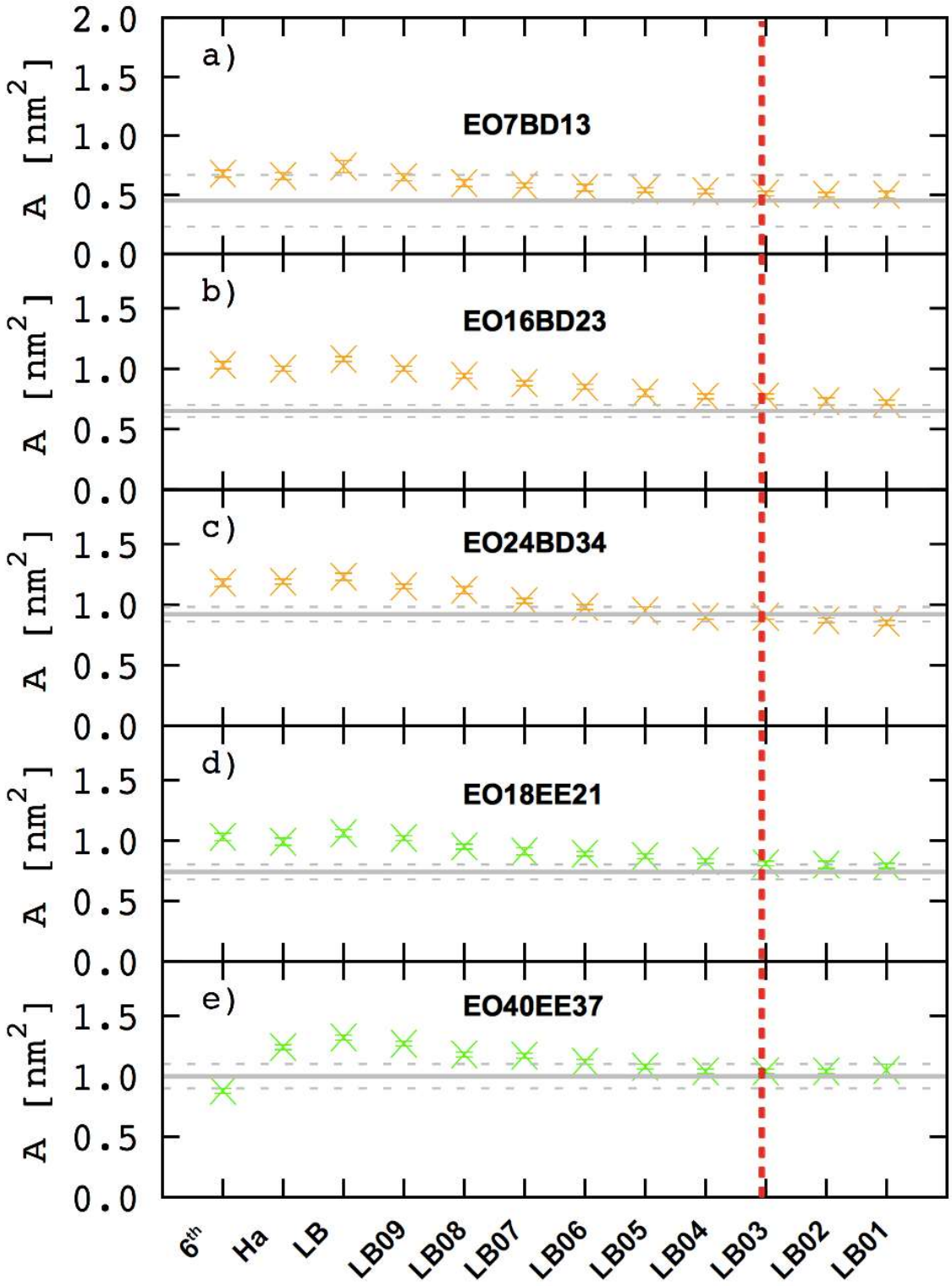

Figure S9: Comparison of area/chain values for simulations and experiments. Area/chain values from simulations using different combining rules are compared with those calculated from experimental membrane thickness measurements (gray lines, with dashed lines representing experimental uncertainty). The $LB^{0.3}$ scaling rule used to best match the experimental membrane thickness measurements also leads to good agreement for area/chain.

Example calculation for area/chain

Because it is difficult to accurately measure the area/chain of a polymer membrane, this value is commonly calculated from the membrane thickness using the assumption that the polymer is incompressible[2]. First, we obtain the hydrophobic block's molecular volume:

$$V_{chain} = \frac{N_{pho}\ MW_{phob}}{\rho_{phob}} \qquad (S1)$$

Here, N is the number-average degree of polymerization, MW is the monomer molar mass, and ρ is the density (0.9 g/cm^3 for both EE and 1,2-BD). Once we know the volume for a hydrophobic block, we calculate the area using this value and half the thickness of the membrane (measured using cryo-TEM):

$$A = \frac{V_{chain}}{d/2} \qquad (S2)$$

For EO7-BD13, the chain volume is

$$V_{chain} = \frac{(13\ monomers)(54\ Da/monomer)}{(0.9\ g/cm^3)} \frac{1g}{6.02 \times 10^{23}\ Da} \left(\frac{10^9\ nm}{100\ cm}\right)^3 = 1.30\ nm^3$$

And the area/chain is

$$A = \frac{1.30\ nm^3}{(5.4\ nm)/2} = 0.48\ nm^2$$

Example calculation for degree of stretching

To determine the degree of chain stretching, we compare the membrane thickness (obtained either from a cryo-TEM image or simulation) to the end-to-end distance of a random coil with the same degree of polymerization and monomer identity as the block in question (hydrophobic or hydrophilic). This end-to-end distance is

$$< R^2 >^{1/2} = b \left(\frac{M_n}{M_0}\right)^{1/2} \qquad (S3)$$

Where $<R^2>^{1/2}$ is the end-to-end distance, b is the Kuhn length, M_n is the number-average molecular mass, and M_0 is the mass of the Kuhn monomer[3,4]. These values are given in **Table S2**.

Table S2: Kuhn monomer masses and lengths used to calculate the stretching parameter. Data for EE and 1,2-BD are obtained from Fetters and Colby[3], and from Grassley and Douglas[5] for EO.

Monomer	Kuhn Length [nm]	Kuhn Monomer Mass [g/mol]
1,2-butadiene	1.37	284.8
Ethyl ethylene	1.05	230.9
Ethylene oxide	0.8	100

The degree of stretching is then calculated from the membrane thickness as follows:

$$s = \frac{d/2}{< R^2 >^{1/2}} \qquad (S4)$$

For EO7-BD12, we can calculate a 1,2-BD end-to-end distance of

$$< R^2 >^{1/2} = (1.37\ nm)\left(\frac{13 \times 54 \frac{g}{mol}}{284.8 \frac{g}{mol}}\right)^{\frac{1}{2}} = 2.15nm$$

Using the thickness 4.7 nm that we obtain from our CG model for 1,2-BD, we calculate a degree of stretching

$$s = \frac{(4.7\ nm)/2}{2.15\ nm} = 1.09$$

Comparison of the EO corona to a grafted polymer brush

Because the EO chains in our BC membranes are tightly packed in the plane of the membrane (A/chain is 9-26% of the value for a random coil, $A_0 \sim <R^2> = Nb^2$), we expect that the EO corona will have a structure with parallels to that of a densely packed polymer brush[4,6]. Using the scaling theory developed by Alexander and De Gennes, we can predict the order of magnitude for the corona thickness[6-8]:

$$h = N(w\sigma b^2)^{1/3} \qquad (S5)$$

Here, h is the brush height, N is the number of Kuhn monomers, b is the Kuhn length, σ is the grafting density (A/chain^{-1}), and w is the excluded volume parameter given by[4]

$$w = -\int_0^\infty \left(1 - e^{-\frac{U(r)}{kT}}\right) d^3r \qquad (S6)$$

Where U(r) is the LJ9-6 potential for CG EO given in **Table 3**, k is Boltzmann's constant, T is temperature, and d^3r indicates integration over three-dimensional space. In **Figure S10**, we show that our EO coronas follow the same scaling behavior as an Alexander-De Gennes brush by plotting $h\sigma^{-1/3}$ as a function of N. This plot yields a straight line with slope 0.31, which is on the same order of magnitude as the slope $(wb^2)^{1/3} = [(0.214\ nm^3) \times (0.8\ nm)^2]^{1/3} = 0.52\ nm^{5/3}$ that we would predict from equation S5.

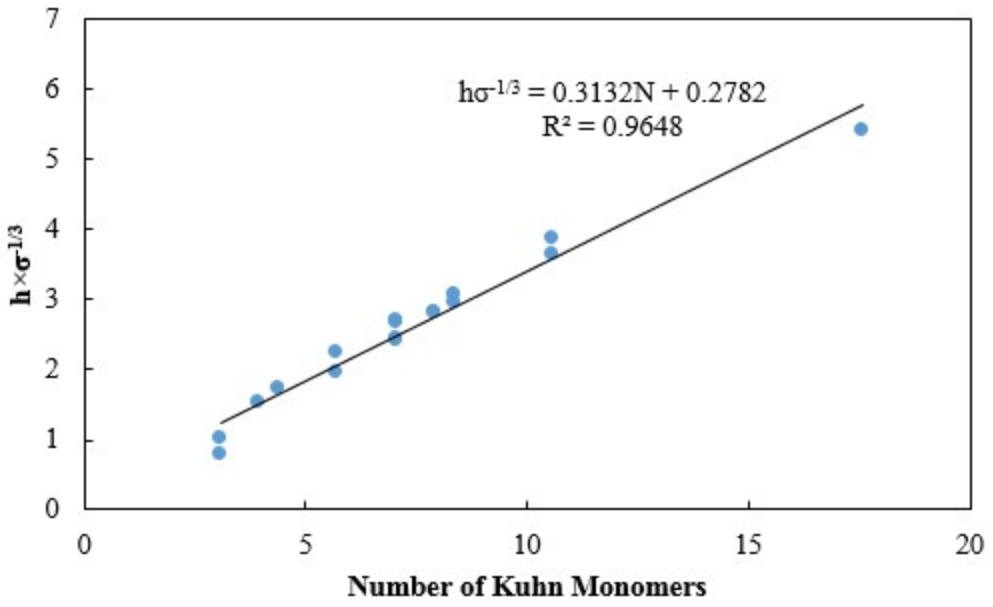

Figure S10: Comparison of EO corona thickness scaling to that expected for a tethered polymer brush. Using equation S5, we can show that the brush thickness h divided by the cube root of the grafting density σ should be directly proportional to the number of Kuhn monomers N.

Based on this scaling analysis, we can confirm that our EO coronas behave similarly to stretched polymer brushes. **Table S3** contains the data needed to prepare **Figure S10**, as well as a comparison of the brush thicknesses obtained from our simulations and predicted using the Alexander-De Gennes theory.

Table S3: Comparison of the EO corona to a tethered EO polymer brush. N_{EO} is the number of EO Kuhn monomers, R is the random coil end-to-end distance, s is the degree of EO chain stretching, σ is the grafting density, and h is the corona thickness (from simulation or predicted using the Alexander-De Gennes theory (ADG)).

Polymer	N_{EO}	A/chain [nm^2]	$<R^2>$ [nm^2]	s	σ [chain/nm^2]	h [nm] (ADG)	h [nm] (simulation)	hsim/hADG	$h\sigma^{-1/3}$
EO7BD13	3.1	0.51	2.0	0.7	2.0	2.0	1.0	0.49	0.8
EO10BD9	4.0	0.59	2.5	1.1	1.7	2.4	1.8	0.74	1.5
EO13BD12	5.7	0.66	3.7	1.2	1.5	3.4	2.2	0.66	2.0
EO16BD15	7.0	0.73	4.5	1.3	1.4	4.0	2.7	0.66	2.4
EO19BD18	8.4	0.80	5.4	1.4	1.3	4.6	3.2	0.68	2.9
EO18BD21	7.9	0.73	5.1	1.4	1.4	4.5	3.1	0.69	2.8
EO16BD23	7.0	0.77	4.5	1.3	1.3	4.0	2.7	0.67	2.4
EO24BD34	10.6	0.90	6.8	1.5	1.1	5.6	3.8	0.67	3.6
EO7EE13	3.1	0.57	2.0	0.9	1.8	1.9	1.2	0.64	1.0
EO10EE9	4.4	0.64	2.8	1.2	1.6	2.6	2.0	0.76	1.7
EO13EE12	5.7	0.72	3.7	1.3	1.4	3.3	2.5	0.76	2.2
EO16EE15	7.0	0.80	4.5	1.4	1.3	3.9	2.9	0.74	2.7
EO19EE18	8.4	0.83	5.4	1.4	1.2	4.6	3.3	0.72	3.1
EO18EE21	7.9	0.81	5.1	1.3	1.2	4.4	3.0	0.69	2.8
EO16EE23	7.0	0.82	4.5	1.3	1.2	3.9	2.9	0.74	2.7
EO24EE34	10.6	1.0	6.8	1.5	1.0	5.5	3.9	0.71	3.9
EO40EE37	17.6	1.0	11.3	1.6	1.0	9.0	5.3	0.60	5.4

Determination of polymer membrane thickness via cryogenic transmission electron microscopy (cryo-TEM)

We synthesized EO-EE and EO-1,2-BD polymers via anionic polymerization and determined their molecular weights and polydispersities via NMR and GPC. Polymer vesicles were then prepared via the film rehydration method[9], and membrane images were made using cryo-TEM. Details of the cryo-TEM sample preparation and measurement methods are given in the Supporting Information for one of our previous papers[10], and the synthesis procedures used are based on those of Hillmyer *et al*[11]. To synthesize EO-1,2-BD rather than EO-EE block copolymers, we skipped the hydrogenation step used to convert 1,2-BD to EE (step 2 in Scheme 1 of Hillmyer's paper)[11]. Using ImageJ software[12], we measured the membrane thicknesses for a number of vesicles (at least 30 vesicles for each polymer) and made three membrane thickness measurements at different points around the circumference of each vesicle. By calculating the average and standard and deviation for all measurements, we determined the membrane thickness for each polymer we synthesized. Our work for EO18-EE21 is shown below as an example, and the same procedure was used for EO7-BD13, EO16-BD23, and EO24-EO34. **Figure S11** shows a membrane thickness measurements made for one cryo-TEM image, while **Table S4** shows the thicknesses for all images examined.

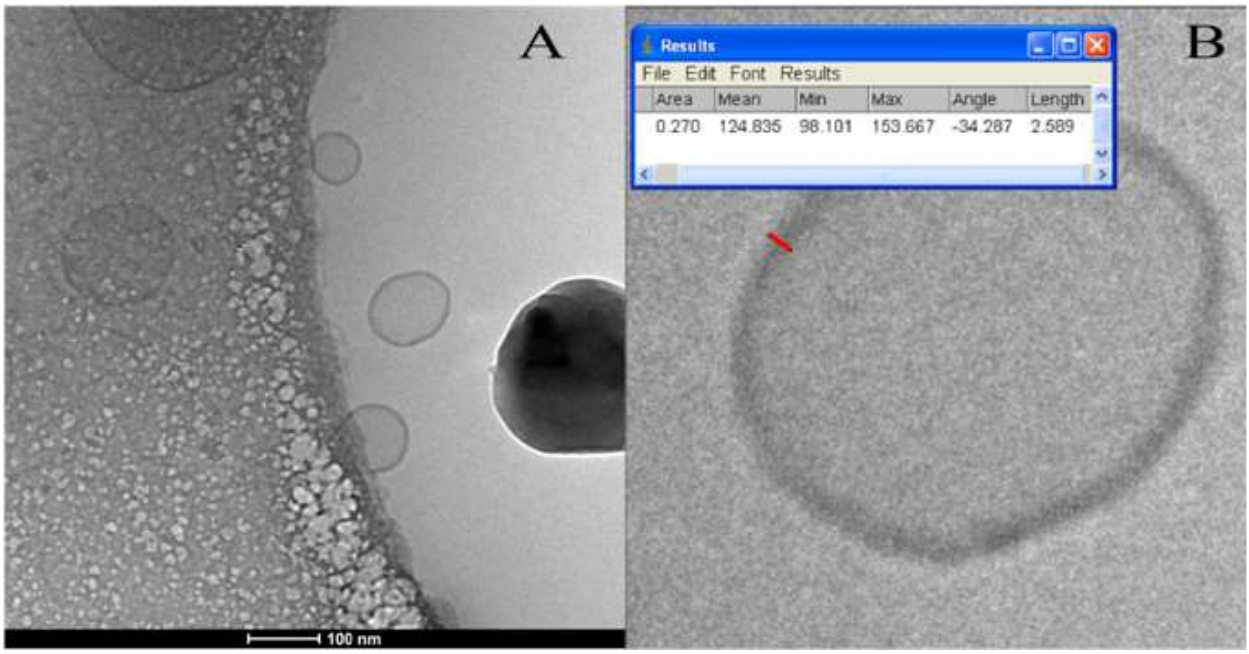

Figure S11: Determination of polymer membrane thickness based on cryo-TEM. A cryo-TEM image shows several EO18-EE21 vesicles (A). Using ImageJ software, we measured membrane thicknesses (in pixels) at several points on each vesicle. One such measurement on the middle vesicle from (A) is shown in (B). We measured the length of the scale bar (48 pixels = 100 nm) to place these thickness measurements on an absolute scale.

Table S4: EO18-EE21 membrane thickness measurements from cryo-TEM. Using measurements from a number of vesicle images, we determined the average EO18-EE21 membrane thickness and its standard deviation.

	membrane thickness			membrane thickness			membrane thickness	
Vesicle	Pixels	nm	Vesicle	Pixels	nm	Vesicle	Pixels	nm
1	3.5	7.2	13	3.3	6.8	25	4.0	8.3
	3.9	8.1		2.4	5.0		2.9	6.0
	2.8	5.9		2.8	5.8		3.0	6.2
2	2.6	5.4	14	2.1	4.4	26	2.6	5.3
	2.7	5.7		2.7	5.7		2.8	5.8
	2.8	5.8		2.2	4.7		3.0	6.3
3	2.9	6.0	15	2.8	5.9	27	3.8	7.9
	2.1	4.4		2.1	4.4		2.7	5.6
	3.0	6.3		2.4	5.1		3.0	6.3
4	3.4	7.1	16	3.1	6.4	28	2.9	6.0
	2.0	4.1		2.6	5.4		2.9	6.0
	2.1	4.3		2.6	5.4		2.4	5.0
5	3.0	6.3	17	3.4	7.2	29	2.8	5.8
	1.9	3.9		3.4	7.2		2.2	4.5
	2.6	5.4		2.4	5.0		2.8	5.8
6	2.8	5.8	18	3.0	6.2	30	2.8	5.9
	3.5	7.3		2.2	4.5		3.6	7.4
	3.3	6.9		2.0	4.1		2.4	5.0
7	3.7	7.7	19	3.7	7.7	31	2.5	5.3
	3.6	7.5		2.5	5.2		2.6	5.4
	3.0	6.3		2.4	5.1		2.7	5.7
8	3.2	6.7	20	3.8	7.8	32	2.3	4.7
	2.4	5.0		3.4	7.1		1.3	2.8
	2.8	5.9		2.9	6.0		2.9	6.0
9	2.2	4.7	21	3.1	6.4	33	2.3	4.9
	3.1	6.5		1.9	4.0		2.6	5.4
	2.3	4.8		2.5	5.3		2.8	5.8
10	2.1	4.4	22	4.0	8.3	34	3.8	8.0
	2.9	6.0		3.6	7.5		3.3	6.9
	2.4	5.0		3.1	6.5		2.5	5.3
11	2.3	4.7	23	2.6	5.4	35	3.5	7.3
	2.4	5.0		2.4	5.0		3.1	6.5
	2.2	4.5		2.8	5.8		3.2	6.6
12	2.4	5.0	24	3.8	7.9			
	3.0	6.2		2.7	5.6	Average		5.9
	2.3	4.7		4.1	8.4	Standard Deviation		1

Works Cited:

(1) Discher, D. E.; Eisenberg, A. Polymer vesicles, *Science* **2002**, *297*, 967.

(2) Won, Y.-Y.; Brannan, A. K.; Davis, H. T.; Bates, F. S. Cryogenic transmission electron microscopy (Cryo-TEM) of micelles and vesicles formed in water by poly (ethylene oxide)-based block copolymers, *J. Phys. Chem. B* **2002**, *106*, 3354.

(3) Fetters, L.; Lohse, D.; Colby, R. In *Physical properties of polymers handbook*; Springer: 2007, p 447.

(4) Rubinstein, M.; Colby, R. H. *Polymer physics*; OUP Oxford, 2003.

(5) Graessley, W. W.; Douglas, J. F. Polymeric Liquids and Networks: Structure and Properties, *Phys. Today* **2005**, *58*, 64.

(6) Milner, S. Polymer brushes, *Science* **1991**, *251*, 905.

(7) Alexander, S. Adsorption of chain molecules with a polar head a scaling description, *Journal de Physique* **1977**, *38*, 983.

(8) de Gennes, P. Conformations of polymers attached to an interface, *Macromolecules* **1980**, *13*, 1069.

(9) Kumar, M.; Grzelakowski, M.; Zilles, J.; Clark, M.; Meier, W. Highly permeable polymeric membranes based on the incorporation of the functional water channel protein Aquaporin Z, *Proc. Natl. Acad. Sci.* **2007**, *104*, 20719.

(10) Schantz, A. B.; Saboe, P. O.; Sines, I. T.; Lee, H.-Y.; Bishop, K. J.; Maranas, J. K.; Butler, P. D.; Kumar, M. PEE–PEO Block Copolymer Exchange Rate between Mixed Micelles Is Detergent and Temperature Activated, *Macromolecules* **2017**, *50*, 2484.

(11) Hillmyer, M. A.; Bates, F. S. Synthesis and characterization of model polyalkane-poly (ethylene oxide) block copolymers, *Macromolecules* **1996**, *29*, 6994.

(12) Abràmoff, M. D.; Magalhães, P. J.; Ram, S. J. Image processing with ImageJ, *Biophotonics international* **2004**, *11*, 36.